RSC Advances

PAPER

Cite this: *RSC Adv.*, 2021, **11**, 15477

Readily-fabricated supported MgO catalysts for efficient and green synthesis of diethyl carbonate from ethyl carbamate and ethanol

Fengjiao Li, *[ab] Liguo Wang, *[c] Shuang Xu,[c] Shuting Liang[d] and Ningning Zhang[a]

Received 20th February 2021
Accepted 18th April 2021

DOI: 10.1039/d1ra01386f

rsc.li/rsc-advances

Developing cost-effective, high-efficiency and heterogeneous catalysts is of prime importance for the green synthesis of diethyl carbonate (DEC) from ethyl carbamate (EC) and ethanol. Herein, a series of MgO/γ-Al_2O_3 catalysts were readily fabricated by an impregnation method for DEC synthesis from EC and ethanol. The activities of the as-prepared MgO/γ-Al_2O_3 catalysts as well as the individual MgO or γ-Al_2O_3 were first tested in the batch reactor. Among the investigated samples, the MgO/γ-Al_2O_3 with a MgO loading of 10 wt% (denoted as 10% MgO/γ-Al_2O_3) exhibited the largest amount of stronger basic sites, and the highest activities with EC conversion of 41.8% and DEC yield of 30.4%, respectively. Furthermore, the DEC yield was greatly boosted to 52.1% with a high DEC selectivity of 93.8% over the 10% MgO/γ-Al_2O_3 catalyst under the optimized reaction conditions in the fixed bed reactor, outperforming most of the reported catalysts.

1. Introduction

Diethyl carbonate (DEC) is an important linear carbonate in the 21st century, which can be widely used as a carbonylating reagent, alkylating reagent, solvent, electrolyte, fuel additive, *etc.*[1–3] Various methods have been adopted to produce DEC. The earliest one is the phosgenation of ethanol to synthesize DEC in 1941, which involved an extremely hazardous raw material such as phosgene.[4] To avoid the usage of the poisonous phosgene, a number of phosgene-free routes such as transesterification of carbonate,[5–8] carbonation of ethanol,[9,10] coupling reaction from CO_2, epoxides and ethanol,[11] ethanolysis of CO_2,[12–16] ethanolysis of urea,[17–24] and ethanolysis of ethyl carbamate (EC)[24–33] have been developed in the past years. It is worth noting that ethanolysis of urea or EC to produce DEC, which is considered as indirect utilization of CO_2 to high value-added products, has been attracting wide attention and interest in the recent years.

As shown in eqn (1) and (2), ethanolysis of urea to DEC actually occurs in two steps: (i) ethanolysis of urea to EC intermediate and NH_3 by-product, (ii) ethanolysis of EC intermediate to DEC product and NH_3 by-product. The latter one is well known as the rate-determining step, which has dominant impacts on DEC synthesis and strongly calls for the development of efficient catalysts. Urea is easy to decompose at high reaction temperatures, usually causing unsatisfactory DEC yield and selectivity *via* direct ethanolysis of urea. However, the more stable EC intermediate can be easily prepared by ethanolysis of urea with high yield and selectivity even without any catalysts.[17] Therefore, ethanolysis of EC is a more economical and promising route for large-scale production of DEC when compared with the direct ethanolysis of urea to DEC.

(1)

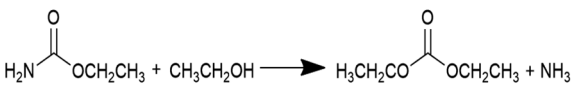

(2)

The ethanolysis of EC to DEC is very sluggish, and the obtained DEC yield under conventional conditions is usually less than 5% without the presence of catalysts.[26–28,31–33] Actually, the DEC yield could be improved to 22.9% with a DEC selectivity of 48.0% from EC in supercritical ethanol, but the extremely harsh conditions of 573 K and 13.2 MPa will inevitably increase the investment costs on reactors.[12] Therefore, the research work is more focused on developing efficient catalysts for DEC synthesis from EC and ethanol. For instance, Zhao *et al.* applied different transition metal chlorides to investigate the catalysis effects in the batch reactor, and found that the activities

[a]*Shenzhen Automotive Research Institute, Beijing Institute of Technology, Shenzhen 518118, Guangdong, China. E-mail: lifengjiao@szari.ac.cn*

[b]*College of Chemistry and Environmental Engineering, Shenzhen University, Shenzhen 518060, Guangdong, China*

[c]*Key Laboratory for Green Process and Engineering, National Engineering Laboratory for Hydrometallurgical Cleaner Production Technology, Institute of Process Engineering, Chinese Academy of Sciences, Beijing 100190, China. E-mail: lgwang@ipe.ac.cn*

[d]*College of Chemical and Environmental Engineering, Chongqing University of Arts and Sciences, Yongchuan, Chongqing 402160, China*

followed the sequence of $MnCl_2$ > $CoCl_2$ > $ZnCl_2$ > $CdCl_2$ > $NiCl_2$.[33] However, the EC conversion and DEC yield over the highest $MnCl_2$ is only 23% and 11%, respectively. In addition, these transition metal chlorides were homogeneous and normally suffered from the difficulties in separating from the products. In contrast, single or mixed metal oxides such as PbO,[25] ZnO[24] and zinc-based mixed oxides (*e.g.*, ZnO–PbO,[26] and Zn–Al–M based oxides (M = Ca, Mg, La and Y)[30]), MgO[28] and magnesium-based mixed oxides (*e.g.*, waste slag derived oxides,[27] transition metal-modified mesoporous Mg–Al mixed oxides,[29] and Mg–Al–Y mixed oxides[31]), and CeO_2 [32] were more frequently employed in the batch reactors. In general, the DEC yields over the Pb-containing oxides are lower than 21%.[25,26] In addition, the post-treatment of the non-environment-friendly Pb element is another challenge for green and large-scale synthesis of DEC. As for the single ZnO or ZnO-containing mixed oxides, the ZnO component was converted to the homogenous $Zn(NH_3)_2(NCO)_2$ during the reaction, which functioned as the real active composition for DEC synthesis,[24,26] and thus would also lead to the problems of separating catalysts. Recently, the Mg-containing oxides have shown great potentials as heterogenous catalysts for efficient DEC synthesis in the batch reactors.[27–29,31] It was discovered that the activity of MgO is strongly dependent on the preparation method, and the MgO nanosheet (MgO-SC-450) exhibited the highest catalytic activities among the investigated MgO samples prepared by different methods.[28] However, these methods to obtain MgO-based materials appear to be expensive and complicated for practical applications of DEC synthesis. Furthermore, the mechanical strength of MgO is relatively low, and shaping of MgO-based materials is also complex. It can be also noted that the above-mentioned catalysts were used in the batch reactors. Therefore, it still remains a formidable challenge to develop highly effective, low-cost, and readily-fabricated MgO-based catalysts with strong mechanical strength for continuous synthesis of DEC *via* ethanolysis of EC in the fixed bed reactors.

In this work, using the common γ-Al_2O_3 with strong mechanical strength as the support, a series of MgO/γ-Al_2O_3 catalysts with different MgO loadings (*e.g.*, 5 wt%, 10 wt% and 15 wt%) were readily prepared by a facile impregnation method for the synthesis of DEC from EC and ethanol. The structures and physiochemical properties of the above supported catalysts, the γ-Al_2O_3 support and the pure MgO sample were systematically characterized by X-ray diffraction (XRD), X-ray photoelectron spectra (XPS), field-emission scanning electron microscope (FE-SEM), Fourier transform infrared (FTIR) spectra, N_2 sorption, and temperature programmed desorption of CO_2 (CO_2-TPD). The screening and reusability of catalysts was first evaluated in the batch reactor. Afterwards, the effects of reaction conditions on the performances over the most active catalyst were investigated in the fixed bed reactor for continuous synthesis of DEC from EC and ethanol. This work provides a comprehensive insight into a very cost-effective and highly efficient heterogeneous catalyst system of MgO/γ-Al_2O_3 for continuously manufacturing DEC *via* the reaction of EC and ethanol.

2. Experimental

2.1 Materials

EC (≥98.0% purity), ethanol (99.7% purity), cyclohexanol (≥ 99.0% purity), $Mg(NO_3)_2 \cdot 6H_2O$ (≥99.0% purity) and quartz sand (20–40 mesh) were commercially purchased from Sinopharm Chemical Reagent Co., Ltd., China. γ-Al_2O_3 (20–40 mesh) was obtained from Aladdin Industrial Corporation, China.

2.2 Catalyst preparation

The γ-Al_2O_3 was pre-treated at 873 K for 2 h prior to use. Various MgO supported on γ-Al_2O_3 catalysts with different MgO loadings of 5 wt%, 10 wt%, and 15 wt% were prepared by an impregnation method. First, the γ-Al_2O_3 support was impregnated with a desired amount of magnesium nitrate solution for 18 h at room temperature, followed by drying at 383 K for 12 h and calcination in air at 673 K for 3 h. The obtained catalysts were denoted as 5% MgO/γ-Al_2O_3, 10% MgO/γ-Al_2O_3 and 15% MgO/γ-Al_2O_3, respectively. Pure MgO employed in this paper was also prepared by calcining $Mg(NO_3)_2 \cdot 6H_2O$ at 673 K in air for 3 h for comparison.

2.3 Catalyst characterization

X-ray diffraction (XRD) patterns were acquired with a PANalytical Empyrean diffractometer using Cu Kα radiation at 40 kV, 40 mA.

Field-emission scanning electron microscopy (FE-SEM) images were collected on an FEI Quanta 250 FEG microscope.

X-ray photoelectron spectra (XPS) tests were conducted on an ESCALAB 250Xi spectrometer with Al Kα radiation (1486.6 eV). The C 1 s peak at 284.8 eV was applied as a reference to calibrate all the peaks.

Fourier transform infrared (FTIR) spectra were recorded on a Tensor 27 Fourier-transform infrared spectrometer from 4000 to 400 cm^{-1}.

N_2 sorption analysis experiments were carried out on a Quantachrome Autosorb-1 instrument at 77 K. Prior to the measurements, all the samples were outgassed in vacuum at 573 K for 3 h. The specific surface areas (S_{BET}) of the samples were determined using the N_2 adsorption data at a relative pressure (P/P_0) from 0.05 to 0.30 according to the Barrett–Emmett–Teller (BET) method. The total pore volume (V_P) and the average pore diameter (D_p) of the samples were obtained by analyzing the desorption branch of the isotherms based on the Barrett–Joyner–Halenda (BJH) model.

The CO_2 temperature program desorption (CO_2-TPD) experiments were performed on an AutoChem II 2920 with a thermal conductivity detector (TCD). Typically, the sample was preheated in helium (25 mL min^{-1}) at 393 K for 60 min, and then cooled to 323 K. Afterwards, the sample was saturated with a mixture of 10 vol% CO_2/He (25 mL min^{-1}) for 1 h. The physically-adsorbed CO_2 was removed by flushing with helium (25 mL min^{-1}) at 323 K for 30 min. Finally, the temperature was increased to 923 K at a heating rate of 10 K min^{-1}.

2.4 Catalytic tests

2.4.1 DEC synthesis in the batch reactor. The reactions in the batch reactor were conducted in a 100 mL-stainless-steel autoclave with a magnetic stirrer and a temperature controller. A typical reaction procedure is as follows: first, 34 mmol of EC, 0.34 mol of ethanol, and 10 wt% catalyst (based on the weight of EC) were added into the autoclave. Then the autoclave was sealed, heated to 473 K and retained at 473 K for 3 h under vigorous stirring. After the reaction was finished, the autoclave was cooled to room temperature and depressurized. After the catalyst was separated by centrifugation, the resulting liquid mixtures with cyclohexanol as the internal standard were analyzed on GC-2014 (Shimadzu, Japan) with an Rtx-5 capillary column (30 m × 0.25 mm × 0.25 μm), an autosampler and a flame ionization detector (FID). For the recycling experiments, the used catalyst was separated by centrifugation, washed thoroughly with ethanol, and directly added into the autoclave with fresh EC and ethanol for the next cycle. For clarity, the 10% MgO/γ-Al_2O_3 catalyst after the fifth cycle was denoted as 10% MgO/γ-Al_2O_3-reused. The EC conversion (shorted as EC conv.), DEC yield, DEC selectivity (shorted as DEC sel.) and the yield of *N*-ethyl ethyl carbamate (NEEC) were calculated according to the previous literature.[28]

2.4.2 DEC synthesis in the fixed bed reactor. Continuous synthesis of DEC *via* ethanolysis of EC was carried out in a bench-scale fixed bed reactor with a single stainless-steel tube. The length and inner diameter of the tube are 0.90 m and 1.2 × 10^{-2} m, respectively. The reactor was heated to the desired reaction temperature by three independently controlled tubular furnaces. The reactor was provided with mass flow controllers, pressure indicator, controller devices and four thermocouples to measure the temperatures at four different points. A stuff storage vessel of 3 L capacity was connected to the constant-flux pump through a volumetric buret to measure the liquid flow rate, followed by a preheater. The pump possessed a maximum capacity of 1.2 × 10^{-4} m^3 h^{-1} under a pressure of 200 bar. The product stuff storage vessel of 3 L capacity was connected to the other end of the reactor through a product condenser, which also functioned as a separator for products.

Typically, 2.0 g catalyst (20–40 mesh, about 2.6 mL) was charged into the fixed bed reactor and the residue zone of the reactor was filled with quartz sand (20–40 mesh). Then, the reactor was heated to the expected reaction temperature after being pressured with N_2 to the desired pressure. Afterwards, the solution containing EC and ethanol was continuously introduced into the reactor after being pre-heated to 333 K. After the reaction was finished, the products were cooled in a product condenser at 323 K, in order to avoid the formation of ammonium carbonate from the reaction of carbon dioxide and ammonia. Simultaneously, at the top of the condenser, the gas products were released through the pipeline. The liquid products were introduced into the product storage vessel at the bottom of the condenser. Liquid samples were analyzed by the method similar to those in the batch reactor.

3. Results and discussion

3.1 Catalyst characterization

3.1.1 XRD and XPS. Fig. 1a and b shows XRD patterns of the γ-Al_2O_3 support, the three supported MgO/γ-Al_2O_3 samples,

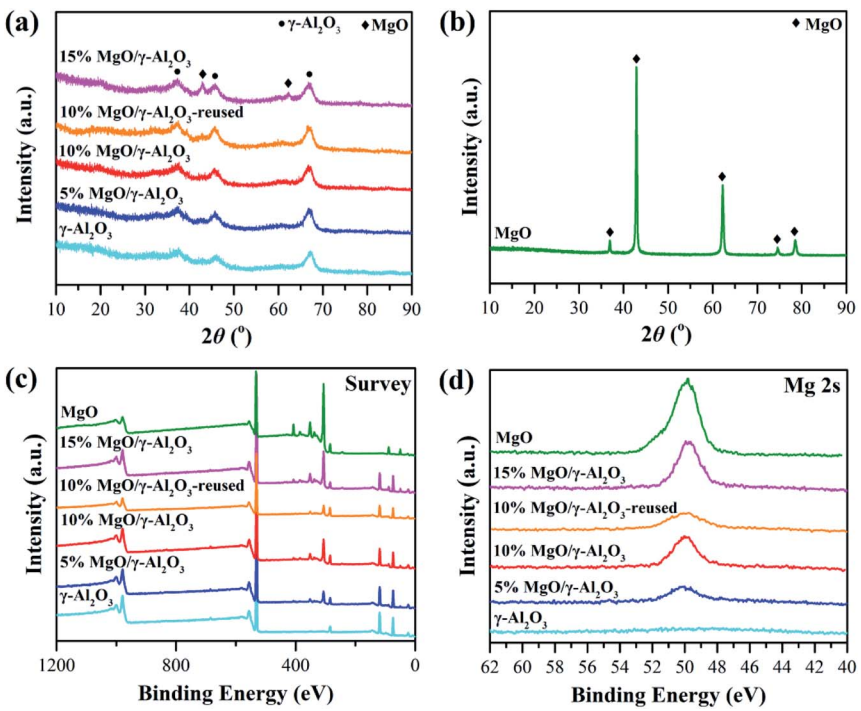

Fig. 1 XRD patterns (a and b), XPS survey spectra (c) and Mg 2s high resolution XPS spectra (d) of the γ-Al_2O_3, 5% MgO/γ-Al_2O_3, 10% MgO/γ-Al_2O_3, 15% MgO/γ-Al_2O_3, MgO and 10% MgO/γ-Al_2O_3-reused samples.

the pure MgO sample and the 10% MgO/γ-Al_2O_3-reused sample. As shown in Fig. 1a, all the MgO/γ-Al_2O_3 samples present the typical diffraction peaks of γ-Al_2O_3 with 2θ values of 37.6°, 45.8° and 67.3° (JCPDS 01-1308). In addition, when the MgO loading is lower than 10 wt%, no crystalline phase of MgO can be found in the 5% MgO/γ-Al_2O_3 and 10% MgO/γ-Al_2O_3 samples, suggesting that MgO was highly dispersed as a monolayer on the surface of the γ-Al_2O_3 support. In contrast, the peak intensities of the crystalline MgO dramatically increases with the MgO loading increasing to 15 wt%, as evidenced by the distinct diffraction peaks of the crystalline MgO in the 15% MgO/γ-Al_2O_3 sample. It was reported that MgO can react with γ-Al_2O_3 to generate Mg–Al spinel when the calcination temperature is higher than 843 K, while no obvious reaction occurs between MgO and γ-Al_2O_3 at a lower calcination temperature of 723 K.[34] Therefore, the reaction of MgO with γ-Al_2O_3 to Mg–Al spinel can be neglected in all the three supported MgO/γ-Al_2O_3 samples, as those supported samples were obtained at a relatively lower calcination temperature of 673 K in this work. Highly crystallized MgO was obviously obtained by calcining $Mg(NO_3)_2 \cdot 6H_2O$ at 673 K in air, as proved by the typical diffraction peaks of MgO (JCPDS 79-0612) in the pure MgO sample (Fig. 1b). The following XPS results (Fig. 1c and d) confirmed that MgO was highly enriched on the surfaces of the MgO/γ-Al_2O_3 samples, also proving that no Mg–Al spinel formed in the three supported MgO/γ-Al_2O_3 samples.

3.1.2 SEM. Fig. 2 presents the SEM images of the γ-Al_2O_3 support, the three supported MgO/γ-Al_2O_3 samples, the pure MgO sample and the 10% MgO/γ-Al_2O_3-reused sample. As presented in Fig. 2a, the pure MgO sample is composed of nanoplates with a thickness of *ca.* 0.12 μm. The γ-Al_2O_3 support is consisted of stacked nano-sized particles with average sizes of *ca.* 30 nm (Fig. 2b). All the three MgO/γ-Al_2O_3 samples possessed similar morphologies with the γ-Al_2O_3 support, and no obvious nanoplates derived from MgO were found in the above supported MgO samples (Fig. 2c–e), also confirming that MgO was highly dispersed on the surfaces of the γ-Al_2O_3 support.

3.1.3 FTIR. Fig. 3 displays the FTIR spectra of the γ-Al_2O_3 support, the three supported MgO/γ-Al_2O_3 samples, and the pure MgO sample. The absorption band around 1633 cm^{-1} is observed in all the above samples, which is well-known as the H–O–H angle bending vibration band of weakly bound molecular water. As for the three supported MgO/γ-Al_2O_3 samples, two broad bands around 780 and 580 cm^{-1} were detected, which corresponded to Al–O–Al bending mode and Al–O stretching mode, respectively, while the band at ~3470 cm^{-1}

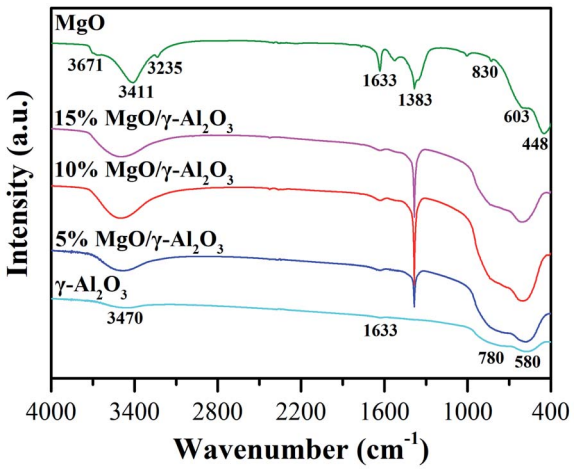

Fig. 3 FTIR of the γ-Al_2O_3, 5% MgO/γ-Al_2O_3, 10% MgO/γ-Al_2O_3, 15% MgO/γ-Al_2O_3 and MgO samples.

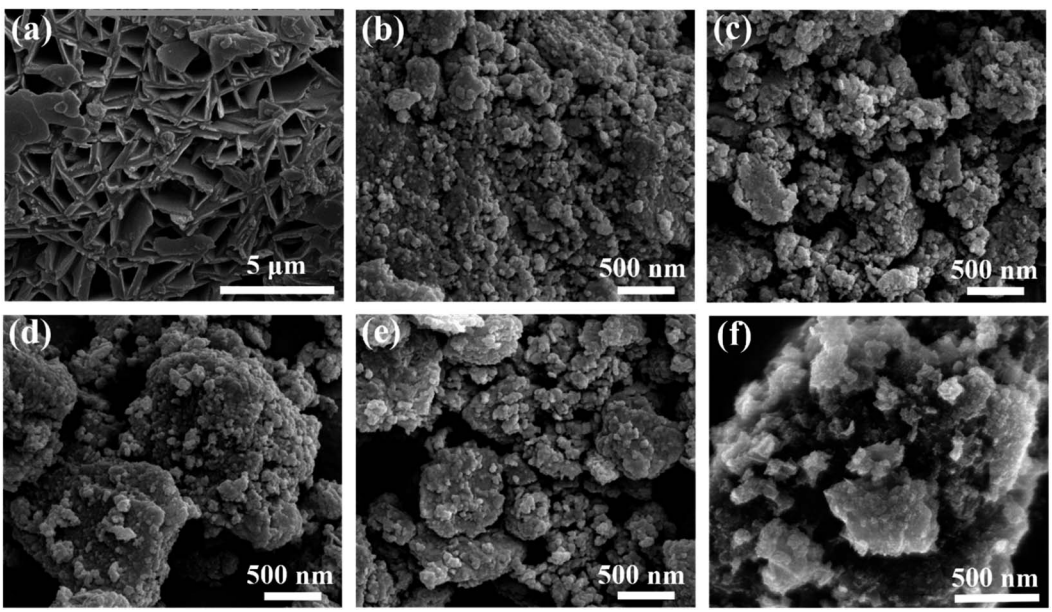

Fig. 2 SEM images of (a) MgO, (b) γ-Al_2O_3, (c) 5% MgO/γ-Al_2O_3, (d) 10% MgO/γ-Al_2O_3, (e) 15% MgO/γ-Al_2O_3 and (f) 10% MgO/γ-Al_2O_3-reused samples.

could be attributed to the presence of the Al–OH bond, all of which are derived from the γ-Al_2O_3 support.[35,36] In addition, the peaks around 1383, 830, 603 and 448 cm^{-1} in all the three supported MgO/γ-Al_2O_3 samples were assigned to the stretching vibration of Mg–O–Mg bonding,[37,38] also confirming the successful formation of MgO on the surfaces of the γ-Al_2O_3 support for the three supported MgO/γ-Al_2O_3 samples.

3.1.4 Nitrogen adsorption/desorption. The N_2 adsorption/desorption isotherms and the corresponding pore size distributions of the γ-Al_2O_3, the three supported MgO/γ-Al_2O_3 and pure MgO samples are shown in Fig. 4, and their corresponding pore structure parameters are summarized in Table 1. As displayed in Fig. 4a, the γ-Al_2O_3 support and the three MgO/γ-Al_2O_3 samples present typical type IV isotherms with obvious hysteresis loops, suggesting that the mesopores of the three MgO/γ-Al_2O_3 samples are derived from the γ-Al_2O_3 support. In addition, the pore sizes of the γ-Al_2O_3 support and the three supported MgO/γ-Al_2O_3 samples mainly center at 7–8 nm (Fig. 4b). As listed in Table 1, the γ-Al_2O_3 support possesses the largest surface area and pore volume (203.0 m^2 g^{-1} and 0.59 cm^3 g^{-1}, respectively) with an average pore diameter of 11.6 nm, while MgO has a negligeable number of pores with the smallest surface area of 5.5 m^2 g^{-1}. After introducing MgO onto the γ-Al_2O_3 support, both the surface areas and pore volumes of the three supported MgO/γ-Al_2O_3 samples decrease with the increasing MgO loadings. However, high specific surface areas (>130 m^2 g^{-1}) and large pore volume (>0.3 cm^3 g^{-1}) are still obtained in the three supported MgO/γ-Al_2O_3 samples due to the high dispersion of MgO on the surface of the γ-Al_2O_3 support.

Table 1 Textural and structural properties of the γ-Al_2O_3, 5% MgO/γ-Al_2O_3, 10% MgO/γ-Al_2O_3, 15% MgO/γ-Al_2O_3 and MgO samples

Sample	S_{BET} (m^2 g^{-1})	V_P (cm^3 g^{-1})	D_p (nm)
γ-Al_2O_3	203.0	0.59	11.6
5% MgO/γ-Al_2O_3	187.5	0.53	11.3
10% MgO/γ-Al_2O_3	167.3	0.46	11.0
15% MgO/γ-Al_2O_3	138.3	0.39	11.2
MgO	5.5	0.02	—

Specifically, the 10% MgO/γ-Al_2O_3 sample possesses a moderate surface area of 167.3 m^2 g^{-1} with a pore volume of 0.46 cm^3 g^{-1} and an average pore diameter of 11.0 nm. The enlarged specific surface areas of the supported MgO/γ-Al_2O_3 samples were beneficial for the active sites to access to the reactants, thus facilitating the enhancement of the EC conversion and DEC yield over the supported MgO/γ-Al_2O_3 samples.

3.1.5 CO_2-TPD. Basic strength and total basicity (*i.e.*, the number of basic sites per unit weight of catalyst) are two crucial parameters to evaluate the basic properties of solid base catalysts.[27,28,31,39] Therefore, to enclose the differences among the γ-Al_2O_3, the three supported MgO/γ-Al_2O_3 and the pure MgO samples, the basic strength and the number of different kinds of basic sites of these oxide catalysts were further investigated by CO_2-TPD. The CO_2-TPD profiles of the above samples are displayed in Fig. 5. In general, the CO_2 desorption peaks represents three kinds of basic sites based on the desorption

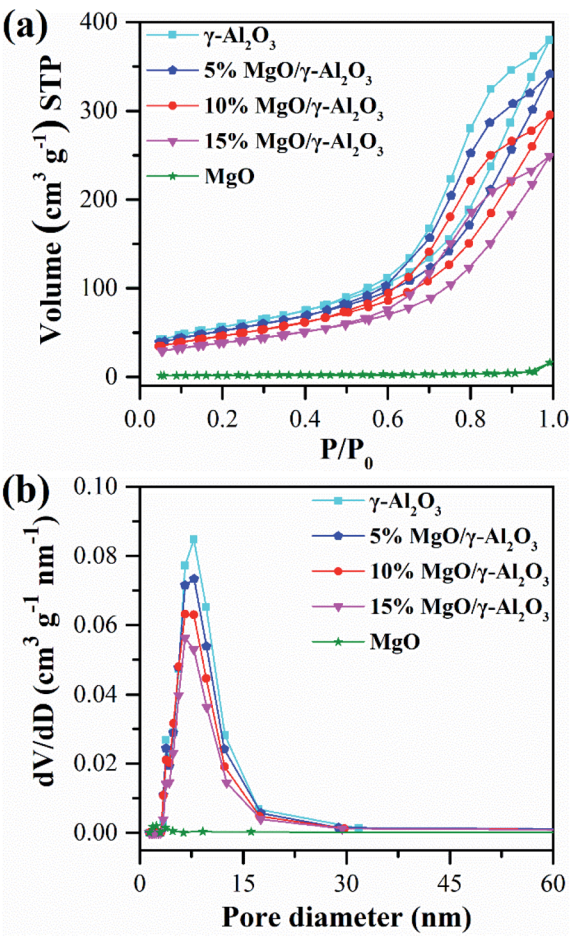

Fig. 4 N_2 adsorption and desorption isotherms (a) and the corresponding pore size distributions (b) of the γ-Al_2O_3, 5% MgO/γ-Al_2O_3, 10% MgO/γ-Al_2O_3, 15% MgO/γ-Al_2O_3 and MgO samples.

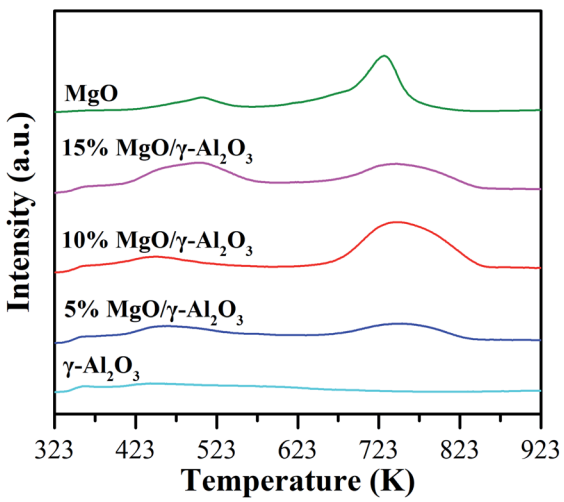

Fig. 5 CO_2-TPD profiles of the γ-Al_2O_3, 5% MgO/γ-Al_2O_3, 10% MgO/γ-Al_2O_3, 15% MgO/γ-Al_2O_3 and MgO samples.

temperatures, *i.e.*, the weak basic sites (CO_2 desorption temperature below 473 K), the medium basic sites (CO_2 desorption temperature between 473 K and 673 K), and the strong basic sites (CO_2 desorption temperature higher than 673 K).[27,31] The corresponding distribution of basic sites on the above samples was listed in Table 2. Among the investigated samples, the γ-Al_2O_3 possessed the lowest amount of total basic sites and strong basic sites (520.5 μmol g^{-1} and 22.1 μmol g^{-1}, respectively), while the pure MgO had the smallest amount of weak basic sites (72.6 μmol g^{-1}) with a moderate amount of medium and strong basic sites. After introducing MgO onto the γ-Al_2O_3 support, the number of total basic sites increased with the increasing MgO loadings, and reached a maximum value of 2196.7 μmol g^{-1} over the 15% MgO/γ-Al_2O_3 sample. In addition, in the region of CO_2 desorption temperature higher than 673 K, the three supported MgO samples definitely required higher temperature for CO_2 to desorb from their surfaces than the pure MgO sample, indicating that the three supported MgO samples possessed stronger basicity in the region of strong basic sites than pure MgO. Importantly, the amount of strong basic sites followed the order of 10% MgO/γ-Al_2O_3 > 15% MgO/γ-Al_2O_3 > 5% MgO/γ-Al_2O_3.

3.2 DEC synthesis in the batch reactor

The performances of the γ-Al_2O_3 support, the three supported MgO catalysts, and the individual MgO sample for DEC synthesis from EC and ethanol were first evaluated in the batch reactor, and the results are summarized in Table 3. The EC conversion and DEC yield over the γ-Al_2O_3 support are 8.3% and 3.6%, respectively (entry 2), which are very close to those in the blank experiment (entry 1), indicating that the γ-Al_2O_3 support was quite inert for DEC synthesis from EC and ethanol. In addition, the pure MgO sample obtained by simple calcination of $Mg(NO_3)_2 \cdot 6H_2O$ at 673 K in air also showed inferior activities towards this reaction (9.5% of EC conversion and 4.0% of DEC yield, entry 6), which is worse than the reported MgO catalysts by thermal decomposition (*i.e.*, MgO-MCBP-450 and MgO-MH-450) and precipitation methods (*i.e.*, MgO-SC-450, MgO-SH-450 and MgO-NH-450),[28] also suggesting that the preparation method had a significant impact on the activities of MgO. However, the three supported MgO/γ-Al_2O_3 catalysts obtained by the facile impregnation method exhibited much higher catalytic abilities than the γ-Al_2O_3 support or the pure MgO sample. As shown in entries 3–5, both the EC conversion and the DEC yield increased with the MgO loading increasing to 10 wt%, and then dropped when the MgO loading was further increased to 15 wt%. It can be clearly found that in the batch reactor, the activities of the supported MgO catalysts follow the similar order with the total amount of strong basic sites. Specifically, the 10% MgO/γ-Al_2O_3 catalyst with the largest total amount of strong basic sites exhibited the highest EC conversion of 41.8% and the highest DEC yield of 30.4%, respectively, while the 5% MgO/γ-Al_2O_3 catalyst with the smallest total amount of strong basic sites showed the lowest activities. The total amount of strong basic sites over the pure MgO sample is close to that over the 5% MgO/γ-Al_2O_3 catalyst, but the activities of the former one is much lower than the latter one, indicating that the high dispersion of MgO on the γ-Al_2O_3 support and the enlarged surface area were also beneficial for the enhanced activities of the supported MgO catalysts. More importantly, the supported MgO catalysts obviously possessed stronger basic sites than the pure MgO sample in the region of desorption temperature higher than 673 K (Fig. 5), therefore, it can be concluded that larger amount of stronger basic sites of the supported MgO catalysts actually played the very crucial role in the DEC synthesis from EC and ethanol.

In a word, the above results suggested that the outstanding activities of the supported MgO catalysts could be attributed to the co-contribution of the high dispersion of MgO on the γ-Al_2O_3 support, the enlarged surface area, and larger amount of stronger basic sites.

The reusability of the 10% MgO/γ-Al_2O_3 catalyst for DEC synthesis in the batch reactor was also investigated for practical application. After the reaction, the catalyst was centrifuged, washed, and directly reused for the next cycle, and the results are shown in Fig. 6. Obviously, the 10% MgO/γ-Al_2O_3 catalyst could be recycled and reused at least five times without significant variation in the activity. Furthermore, XRD, XPS and SEM studies of the 10% MgO/γ-Al_2O_3 catalyst after the fifth cycle (denoted as 10% MgO/γ-Al_2O_3-reused) were also performed, in order to gain a deep insight into the stability of the 10% MgO/γ-Al_2O_3 catalyst. As exhibited in Fig. 1a, compared with the fresh 10% MgO/γ-Al_2O_3 catalyst, there were no obvious changes to the crystallite size and crystal phase after the fifth reuse.

Table 2 The basicities and the distribution of basic sites determined by CO_2-TPD of the γ-Al_2O_3, 5% MgO/γ-Al_2O_3, 10% MgO/γ-Al_2O_3, 15% MgO/γ-Al_2O_3 and MgO samples

	Number of basic sites (μmol g^{-1})			
Sample	Weak	Medium	Strong	Total
γ-Al_2O_3	221.5	276.9	22.1	520.5
5% MgO/γ-Al_2O_3	380.4	538.1	617.1	1535.6
10% MgO/γ-Al_2O_3	270.5	301.9	1054.3	1626.7
15% MgO/γ-Al_2O_3	426.6	881.7	888.4	2196.7
MgO	72.6	334.5	593.2	1000.3

Table 3 The catalytic performances of different catalysts on the DEC synthesis from EC and ethanol in the batch reactor[a]

Entry	Catalyst	EC conv. (%)	DEC yield (%)	DEC sel. (%)	NEEC yield (%)
1	None	6.1	4.4	72.1	—
2	γ-Al_2O_3	8.3	3.6	43.6	1.4
3	5% MgO/γ-Al_2O_3	25.0	10.6	42.5	2.5
4	10% MgO/γ-Al_2O_3	41.8	30.4	72.6	1.6
5	15% MgO/γ-Al_2O_3	32.2	19.3	59.9	2.5
6	MgO	9.5	4.0	41.5	1.3

[a] Reaction conditions: 473 K, 34 mmol of EC, 0.34 mol of ethanol, 10 wt% of catalyst amount (based on the weight of EC), and 3 h.

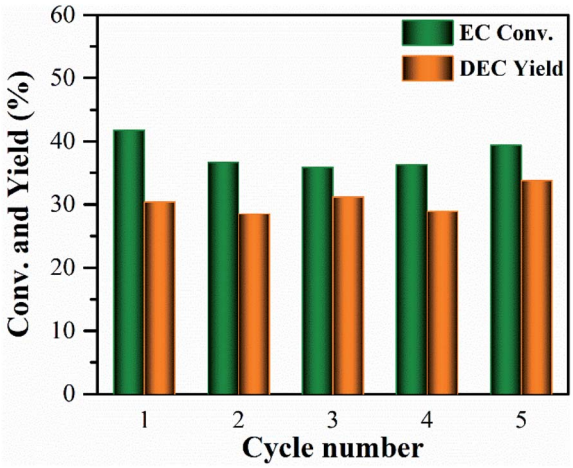

Fig. 6 The reusability of the 10% MgO/γ-Al_2O_3 catalyst for DEC synthesis from EC and ethanol in the batch reactor. Reaction conditions: 473 K, 34 mmol of EC, 0.34 mol of ethanol, 10 wt% of catalyst amount (based on the weight of EC), and 3 h.

XPS also shows no distinct changes between the fresh and the reused 10% MgO/γ-Al_2O_3 catalyst, indicating that no new species were formed after reuse (Fig. 1c and d). In addition, the 10% MgO/γ-Al_2O_3-reused catalyst showed similar morphologies (Fig. 3f) in comparison with the fresh one. Therefore, it could be concluded that the 10% MgO/γ-Al_2O_3 catalyst has a remarkable structure stability and reusability for DEC synthesis from EC and ethanol.

3.3 DEC synthesis in the fixed-bed reactor

Despite of the high activities of the 10% MgO/γ-Al_2O_3 catalyst in the batch reactor, the NH_3 by-product was accumulated in the batch reactor and would restrict the shift of the reaction equilibrium to DEC synthesis, which is disadvantageous to the improvement of DEC yield. Therefore, the performances of the 10% MgO/γ-Al_2O_3 catalyst for continuous synthesis of DEC from EC and ethanol were further investigated in the fixed-bed reactor, which could efficiently shift the reaction equilibrium to the side of DEC synthesis by removing the ammonia by-product simultaneously from the reactor. In addition, this reactor would also alleviate the problems of the undesirable side reactions, thus helping to improve the DEC yield and selectivity.

At first, the experiment only with quartz sand filled into the whole tube of the fixed bed reactor was conducted under the reaction condition of 463 K, 1.6 MPa, EC solution liquid hourly space velocity (LHSV) of 2.02 h^{-1}, and the molar ratio of ethanol to EC (shorted as n(EtOH)/n(EC)) of 10. As shown in Fig. 7a, in the absence of the 10% MgO/γ-Al_2O_3 catalyst, both the EC conversion and the DEC yield are extremely low, which are 3.7%

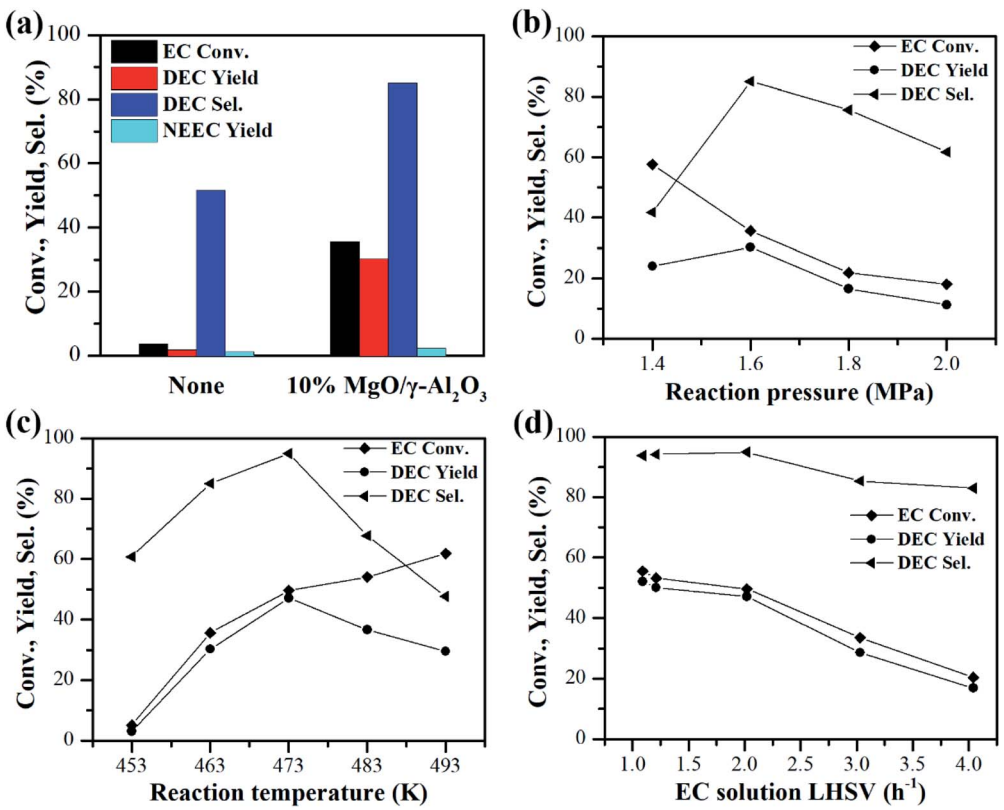

Fig. 7 Effects of reaction conditions on the performances of the 10% MgO/γ-Al_2O_3 catalyst for continuous synthesis of DEC from EC and ethanol in the fixed bed reactor, 2 g of catalyst, n(EtOH)/n(EC) of 10. (a) Comparison before and after the addition of the 10% MgO/γ-Al_2O_3 catalyst. Reaction conditions: 463 K, 1.6 MPa, EC solution LHSV of 2.02 h^{-1}; (b) effect of reaction pressure. Reaction conditions: 463 K, EC solution LHSV of 2.02 h^{-1}; (c) effect of reaction temperature. Reaction conditions: 1.6 MPa, EC solution LHSV of 2.02 h^{-1}; (d) effect of EC solution LHSV. Reaction conditions: 473 K, 1.6 MPa.

and 1.9%, respectively, demonstrating that the quartz sand is inactive towards this reaction. However, after the 10% MgO/γ-Al_2O_3 catalyst was loaded into the reaction zone in the fixed bed reactor, the EC conversion and the DEC yield were greatly boosted to 35.6% and 30.3% under the same reaction conditions, also re-confirming the superior activities of the 10% MgO/γ-Al_2O_3 catalyst (Fig. 7a). Furthermore, the effects of reaction conditions such as reaction pressure, reaction temperature, and EC solution LHSV on the catalytic performances of the 10% MgO/γ-Al_2O_3 catalyst for continuous synthesis of DEC from EC and ethanol in the fixed-bed reactor were also investigated.

The effect of reaction pressure is shown in Fig. 7b. Theoretically, low pressure is beneficial for the ammonia by-product to escape from the reaction system.[40] As a result, the EC conversion gradually increased with the reaction pressure decreasing from 2.0 MPa to 1.4 MPa. However, the DEC yield first increased with the reaction pressure increasing from 1.4 MPa to 1.6 MPa, and then dropped from 1.6 MPa to 2.0 MPa. In addition, 85.0% of DEC selectivity was obtained at 1.6 MPa, which was higher than that in the batch reactor at a higher reaction temperature of 473 K (72.6% of DEC selectivity, entry 4 in Table 3). Therefore, the suitable reaction pressure for the DEC synthesis in the fixed bed reactor should be 1.6 MPa.

The effect of reaction temperature is displayed in Fig. 7c. The EC conversion increased with the reaction temperature increasing from 453 K to 493 K. In contrast, the DEC yield first increased with the reaction temperature increasing from 453 K to 473 K, and then dropped after 473 K. As disclosed by previous work, DEC could be decomposed into CO_2 and diethyl ether at temperatures of 453–513 K over catalysts.[41] Therefore, the rapid drop of DEC yields from 483 to 493 K is largely ascribed to the decomposition of the DEC to carbon dioxide and diethyl ether at too high temperatures. It should be noted that the maximal DEC yield of 47.1% with a DEC selectivity higher than 90% was achieved at 473 K. Therefore, the optimized reaction temperature for the DEC synthesis in the fixed-bed reactor was 473 K.

The effect of EC solution LHSV on the continuous synthesis of DEC from EC and ethanol over the 10% MgO/γ-Al_2O_3 catalyst was displayed in Fig. 7d. Both the EC conversion and the DEC yield decreased with the EC solution LHSV increasing from 1.09 h^{-1} to 4.04 h^{-1}. A higher EC solution LHSV indicated that a larger amount of EC was used. As the amount of catalyst is constant, the low EC solution LHSV of 1.09 h^{-1} was advantageous to obtain high DEC yield.

It should be noted that under the optimized reaction conditions of 473 K, 1.6 MPa, EC solution LHSV of 1.09 h^{-1}, n(EtOH)/n(EC) of 10, 2 g of 10% MgO/γ-Al_2O_3 catalyst, EC conversion of 55.5%, a maximum DEC yield of 52.1% and a high DEC selectivity of 93.8% were achieved in the fixed bed reactor, which are superior to most of the reported catalysts.[24–27,30,32,33]

The catalytic stability of the 10% MgO/γ-Al_2O_3 catalyst was also tested in the fixed-bed reactor. As presented in Fig. 8, with the reactants continuously pumping into the fixed bed reactor, no obvious changes in EC conversion and DEC yield were observed after 7 h of test over the 10% MgO/γ-Al_2O_3 catalyst, also indicative of the outstanding stability of the 10% MgO/γ-Al_2O_3 catalyst for DEC synthesis from EC and ethanol.

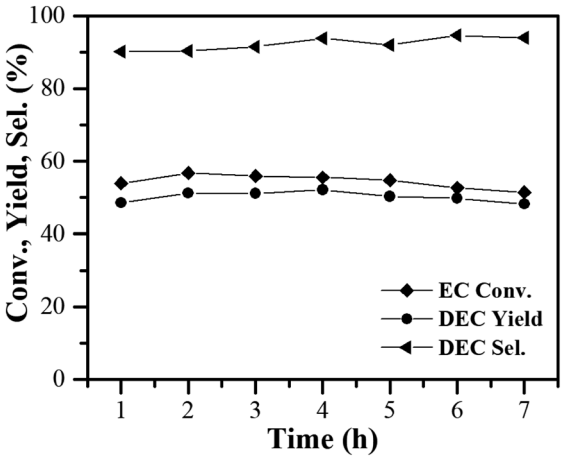

Fig. 8 Continuous synthesis of DEC from EC and ethanol over time using the 10% MgO/γ-Al_2O_3 catalyst. Reaction conditions: 473 K, 1.6 MPa, EC solution LHSV of 1.09 h^{-1}, n(EtOH)/n(EC) of 10, 2 g catalyst.

Based on the above results, it could be concluded that the readily-fabricated 10% MgO/γ-Al_2O_3 catalyst was a very promising candidate as a highly-efficient, cost-effective and heterogenous catalyst for green and continuous synthesis of DEC using low-cost and environmental-benign EC and ethanol as raw materials, which is also an efficient way to indirectly utilize CO_2 to synthesize high value-added chemicals.

4. Conclusions

In this work, low-cost and effective supported MgO catalysts readily fabricated by an impregnation method were employed for green synthesis of DEC from EC and ethanol. The 10% MgO/γ-Al_2O_3 catalyst presented the highest activities in the fixed bed reactor with a maximum DEC yield of 52.1% and a high DEC selectivity of 93.8%, respectively, which are superior to the individual γ-Al_2O_3 or MgO, and most of the reported catalysts. The outstanding performances of the 10% MgO/γ-Al_2O_3 catalyst could be attributed to the co-contribution of the high dispersion of MgO on the γ-Al_2O_3 support, the enlarged surface area, and larger amount of stronger basic sites. This work has provided a readily-fabricated and economical catalyst system to efficiently synthesize high value-added DEC indirectly from CO_2.

Conflicts of interest

There are no conflicts to declare.

Acknowledgements

This work is financially supported by National Natural Science Foundation of China (No. 21706162).

Notes and references

1 K. Shukla and V. C. Srivastava, *RSC Adv.*, 2016, **6**, 32624–32645.

2 K. Shukla and V. C. Srivastava, *Catal. Rev.*, 2017, **59**, 1–43.
3 S. Huang, B. Yan, S. Wang and X. Ma, *Chem. Soc. Rev.*, 2015, **44**, 3079–3116.
4 I. E. Muskat, F. Strain, *US Pat.*, 2379250, 1941.
5 H. Iida, R. Kawaguchi and K. Okumura, *Catal. Commun.*, 2018, **108**, 7–11.
6 S.-J. Wang, S.-H. Cheng, P.-H. Chiu and K. Huang, *Ind. Eng. Chem. Res.*, 2014, **53**, 5982–5995.
7 C. Murugan and H. C. Bajaj, *Fuel Process. Technol.*, 2011, **92**, 77–82.
8 K. Shukla and V. C. Srivastava, *Ind. Eng. Chem. Res.*, 2018, **57**, 12726–12735.
9 H. Wang, Y. Xiang, M. Guo, J. Su, G. Wang, W. Cui and Z. Deng, *Energy Fuels*, 2020, **34**, 8697–8706.
10 S. Huang, P. Chen, B. Yan, S. Wang, Y. Shen and X. Ma, *Ind. Eng. Chem. Res.*, 2013, **52**, 6349–6356.
11 L. Wang, H. Li, S. Xin, P. He, Y. Cao, F. Li and X. Hou, *Appl. Catal., A*, 2014, **471**, 19–27.
12 L.-C. Zhao, Z.-Q. Hou, C.-Z. Liu, Y.-Y. Wang and L.-Y. Dai, *Chin. Chem. Lett.*, 2014, **25**, 1395–1398.
13 B.-Y. Yu, P.-J. Wu, C.-C. Tsai and S.-T. Lin, *J. CO_2 Util.*, 2020, **41**, 101254.
14 O. Arbeláez, E. Hernández, L.-M. González, F. Bustamante and A.-L. Villa, *Chem. Eng. Technol.*, 2019, **42**, 1135–1143.
15 M. Buchmann, M. Lucas and M. Rose, *Catal. Sci. Technol.*, 2021, **11**, 1940–1948.
16 J. Wang, Z. Hao and S. Wohlrab, *Green Chem.*, 2017, **19**, 3595–3600.
17 S. Xin, L. Wang, H. Li, K. Huang and F. Li, *Fuel Process. Technol.*, 2014, **126**, 453–459.
18 P. Wang, S. Liu, F. Zhou, B. Yang, A. S. Alshammari and Y. Deng, *RSC Adv.*, 2015, **5**, 19534–19540.
19 K. Shukla and V. C. Srivastava, *Fuel Process. Technol.*, 2017, **161**, 116–124.
20 J. Zhang, T. Yan, Y. Yang, J. Sun, Y. Lin and M. Wei, *Chin. J. Catal.*, 2019, **40**, 515–522.
21 A. Angelini, A. Dibenedetto, D. Curulla-Ferré and M. Aresta, *RSC Adv.*, 2015, **5**, 88401–88408.
22 A. Dibenedetto, A. Angelini, M. Aresta, S. Fasciano, M. E. Cucciolito, F. Ruffo, B. M. Aresta, D. Curulla-Ferré and E. De Giglio, *Appl. Catal., A*, 2015, **493**, 1–7.
23 T. Yan, W. Bing, M. Xu, Y. Li, Y. Yang, G. Cui, L. Yang and M. Wei, *RSC Adv.*, 2018, **8**, 4695–4702.
24 W. Zhao, W. Peng, D. Wang, N. Zhao, J. Li, F. Xiao, W. Wei and Y. Sun, *Catal. Commun.*, 2009, **10**, 655–658.
25 L. Guo, X. Zhao, H. An and Y. Wang, *Chin. J. Catal.*, 2012, **33**, 595–600.
26 H. An, X. Zhao, L. Guo, C. Jia, B. Yuan and Y. Wang, *Appl. Catal., A*, 2012, **433**, 229–235.
27 L. Wang, H. Li, S. Xin and F. Li, *Catal. Commun.*, 2014, **50**, 49–53.
28 F. Li, H. Li, L. Wang, P. He and Y. Cao, *Catal. Sci. Technol.*, 2015, **5**, 1021–1034.
29 D. Wang, X. Zhang, C. Liu, T. Cheng, W. Wei and Y. Sun, *Appl. Catal., A*, 2015, **505**, 478–486.
30 K. Shukla and V. C. Srivastava, *Catal. Lett.*, 2017, **147**, 1891–1902.
31 D. Wang, X. Zhang, D. Zhou, S. Liu and W. Wei, *Fuel Process. Technol.*, 2017, **167**, 404–415.
32 Y. Ma, H. Wang, L. Wang and H. Li, *J. Environ. Manage.*, 2019, **232**, 952–956.
33 W. Zhao, D. Feng, J. Nong, G. Cao, X. Liu, Z. Tang and Y. Chen, *React. Kinet., Mech. Catal.*, 2016, **117**, 639–654.
34 D.-e. Jiang, B. Zhao, Y. Xie, G. Pan, G. Ran and E. Min, *Appl. Catal., A*, 2001, **219**, 69–78.
35 J. Gangwar, B. K. Gupta, S. K. Tripathi and A. K. Srivastava, *Nanoscale*, 2015, **7**, 13313–13344.
36 M. Aazza, H. Ahlafi, H. Moussout, C. Mounir, A. Fadel and A. Addad, *J. Environ. Chem. Eng.*, 2020, **8**, 103707–103718.
37 A. Ansari, A. Ali, M. Asif and Shamsuzzaman, *New J. Chem.*, 2018, **42**, 184–197.
38 J. P. Dhal, M. Sethi, B. G. Mishra and G. Hota, *Mater. Lett.*, 2015, **141**, 267–271.
39 H. Hattori, *Appl. Catal., A*, 2015, **504**, 103–109.
40 D. Wang, X. Zhang, W. Wei and Y. Sun, *Chem. Eng. Technol.*, 2012, **35**, 2183–2188.
41 M. Selva, M. Fabris and A. Perosa, *Green Chem.*, 2011, **13**, 863–872.